TRIBOLOGY ADVANCES

Tribol. Adv. (2026) 1: 003
https://cstr.cn/32476.14.trad-20260006
https://doi.org/10.3724/trad-20260006

Original Research Open Access

Predicting the cyclic oil film thickness variation in reciprocating hydrodynamic line contacts

Robert Ian Taylor*

Jost Institute for Tribotechnology, University of Lancashire, Preston PR1 2HE, UK

Received 23 February 2026; Accepted 7 May 2026; Available online 27 July 2026

ARTICLE INFO

Keywords:
Lubrication
Tribology
Squeeze effect
Reciprocating contact

ABSTRACT

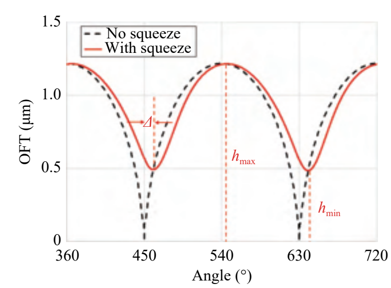

In hydrodynamically lubricated reciprocating contacts, it is well known that the oil film thickness (OFT) is not zero at the reversal points. Calculation of the minimum OFT and the position at which it occurs usually requires a numerical solution of the Reynolds' equation, including "squeeze" effects. Such a model has been developed, and many simulations have been carried out in which the amplitude, slider width, slider radius of curvature, viscosity, oscillation frequency, and applied load have been varied over a wide range. This data has enabled the derivation of useful approximate equations for both the maximum OFT in the contact and the minimum OFT (and its angular position). Knowledge of these three parameters enables fast, reliable predictions of the OFT variation across the entire reciprocating cycle. These results should be useful to users (and manufacturers) of reciprocating tribology test rigs and to those researchers interested in piston ring lubrication.

1. Introduction

Reciprocating contacts are ubiquitous within tribology. For internal combustion engines, piston rings are reciprocating line contacts that are predominantly lubricated hydrodynamically. In addition, the valve trains in engines are elastohydrodynamic reciprocating line contacts. Separately, rolling element bearings often undergo oscillatory motion and are reciprocating elastohydrodynamic point contacts. In addition, many reciprocating test rigs (e.g., the TE 77 [1], the High Frequency Reciprocating Rig (HFRR) [2], Optimol SRV systems [3], and other similar systems from manufacturers such as Bruker Corporation [4] and Rtec Instruments [5]) are used for friction and wear testing within the tribological community.

Useful equations have been proposed to predict the oil film thickness (OFT) in reciprocating contacts. For example, Furuhama and Sasaki [6] has reported that the OFT for a piston ring contact varies in proportion to $\sqrt{\eta U/W}$, where η is lubricant viscosity (Pa·s), U is the relative sliding speed (m/s) of the piston ring with respect to the liner, and W is the load per unit length (N/m) acting on the back of the piston ring.

McGeehan [7] reviewed various equations that purported to predict the minimum OFT in parabolic lubricated line contacts and concluded that the minimum OFT varied according to $(\eta U/W)^x$, where x takes values between 1/3 and 2/3 according to different researchers.

For elastohydrodynamic lubrication, there are well-known equations [8] that are widely used for predicting the minimum and central OFT in a contact. These equations generally use dimensionless quantities, and the appropriate quantity relating to motion contains a term of the form $(\eta U)^{0.7}$.

Therefore, whether lubrication is hydrodynamic or elast-

* Corresponding author.
Robert Ian Taylor, E-mail: ritaylor@lancashire.ac.uk

ohydrodynamic, the simple expressions above, commonly used by tribologists, would predict zero OFT at the reversal points of reciprocating contacts (since the relative sliding speed of the surfaces, U, is zero there).

However, it is known that the OFT at reversal positions, although small, is definitely not zero. This is because the Reynolds' equation [9] includes a term known as the "squeeze" effect. This term allows for pressure generation within the lubricant in the contact when surfaces move normally to each other. Since, in reciprocating contacts, the speed varies from high (at mid-stroke) to zero (at the reversal positions), there is both sliding and normal motion of the contacting surfaces, and it is the "squeeze" effect that is responsible for the non-zero OFT at reversal positions [10–19]. Somewhat surprisingly, despite the enormous interest in reciprocating motion within the tribological community, there are no widely used equations available to tribologists to enable estimation of the minimum OFT in reciprocating hydrodynamically lubricated contacts. The purpose of this work is to report such an equation.

A robust, fast numerical solver (written in Python), which includes "squeeze" effects, has been developed for a simple reciprocating hydrodynamic contact (which assumes a symmetric parabolic slider), and the OFT has been predicted over the full reciprocating cycle and compared to similar calculations that do not include "squeeze" effects. The variation of the minimum OFT with key parameters (such as amplitude and frequency of oscillation, the width of the slider and its radius of curvature, viscosity, and load per unit length acting on the slider) has been explored, and an equation is proposed that will be of use to tribologists wishing to estimate the minimum OFT in such contacts. Since the oil films are expected to be small close to reversal points, the detailed value of the minimum OFT is key to accurately defining the lambda ratio (the ratio of film thickness to surface roughness), which is important for estimating friction and wear around these positions.

The squeeze lubrication problem for contacts moving normally, without any sliding, is considered in many elementary tribology textbooks [9]. In this situation, the aim is usually to calculate the time taken for an oil film trapped between two loaded surfaces to decay from one value to a lower one. There is no sliding, so the "wedge" term in Reynolds' equation is not present, just the "squeeze" term.

"Squeeze" effects for contacts with both normal and sliding motion have primarily been studied for their application to piston ring tribology. Many numerical studies have included "squeeze" effects [10–20], and it has been found that the inclusion of the "squeeze" results in a non-zero OFT close to reversal positions. Most of these "squeeze" studies assumed fully flooded contacts, although some authors have carried out starved analysis [13,18,19]. There have also been useful reviews of piston ring lubrication, in which "squeeze" effects have been discussed [7,21,22], and useful equations proposed for mid-stroke OFT.

In addition, experimental work has been undertaken to investigate the OFT in piston rings close to dead center positions [22–27]. Clearly, the piston ring lubrication problem is quite complex, since (1) the load acting on the ring varies across the cycle (due to the changing combustion pressure in the engine), (2) the viscosity also varies across the cycle (due to a temperature gradient on the liner, from lower temperatures at bottom dead centre (BDC), to higher temperatures at top dead centre (TDC)), (3) the motion of the piston is not a simple sinusoid since the crankshaft links to a con-rod (to convert the rotational motion of the crankshaft to linear motion of the piston), and (4) the top piston ring is usually starved of lubricant, due to the scraping action of the oil control and second ring.

As well as the work referenced above on hydrodynamic reciprocating contacts, it is also worth mentioning that both experimental and theoretical work has been reported for reciprocating elastohydrodynamic contacts [28–34].

In this paper, however, a much simpler reciprocating line contact is considered, in which the motion is purely sinusoidal, the viscosity and load are constant across the cycle, and it is also assumed that the contacting surfaces are smooth and that the contact is fully flooded with lubricant. It is realized that in practical systems, starvation may occur, but a review of the published literature suggests that starvation is most likely to affect the OFT at mid-stroke positions, where the maximum OFT occurs, and since the main focus of the current paper is on the minimum OFT, starvation effects are expected to be less important there. However, it is intended to consider starvation effects in a future publication.

Many numerical simulations have been carried out, and useful equations have been derived that allow tribologists to estimate both the minimum OFT in the contact and its position without the need to run complex computer programs. Potential applications of the equations are also reported for tribological reciprocating test rigs.

2. Analytical method

It is assumed that the position of the center of the slider (with respect to the flat surface), X, varies according to:

$$X = A \sin \omega t, \tag{1}$$

where A is the amplitude (m), ω is the rotational frequency (rad/s), and t is time (s). If f is the frequency of oscillation (s^{-1}), then $\omega = 2\pi f$.

It is useful to define an angle, θ, which is equal to ωt. If "squeeze term" effects are ignored, it would be expected that the OFT would be zero when $\theta = \pm(2N - 1)\pi/2$, where N is an integer, since at these positions, the sliding speed would be zero.

It is assumed that the slider is symmetric, with width b and a parabolic profile $h(x)$.

$$h(x) = h_{\min} + \frac{x^2}{2r}, \tag{2}$$

where $h(x)$ is the height of the contact at position x (m), and $h_{\min}$ is the minimum OFT, which occurs when $x = 0$ (m). The edges of the slider will be at $\pm b/2$.

The slider moves against a flat surface, with a relative speed U:

$$U = \omega A \cos \omega t. \tag{3}$$

The pressure at the inlet to the contact is assumed to be P_1, and that at the outlet is P_2 (both pressures are in units of Pa). The pressure on the back of the contact is assumed to be P_{back}, and the load per unit length acting on the contact is $P_{back} \cdot b$.

A simple separation boundary condition is assumed [35], whereby dP/dx is assumed to be zero at a position x_2, and the pressure at x_2 (and for positions greater than x_2) is equal to P_2.

The situation above is illustrated in Figure 1. It is also assumed throughout the paper that the contact is fully flooded, that lubricant viscosity does not vary with shear rate, and that the surfaces are flat (zero roughness).

The 1D Reynolds' equation can be written as

$$\frac{\partial}{\partial x}\left(\frac{h^3}{12\eta}\frac{\partial P}{\partial x}\right) = \frac{U}{2}\frac{\partial h}{\partial x} + \omega\frac{\partial h}{\partial \theta}, \tag{4}$$

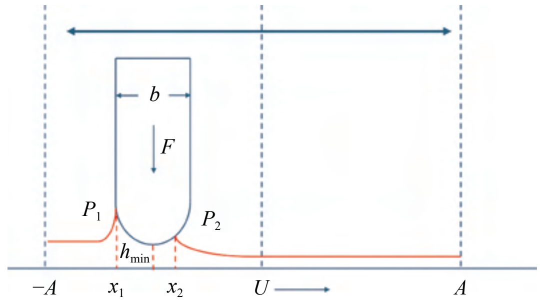

Figure 1 Schematic of reciprocating line contact. The load per unit length acting downwards, F, is equal to $P_{back} \cdot b$, where P_{back} is the pressure on the rear of the slider, and b is the width of the slider.

where $h(x)$ is the variation of contact film thickness with position x, $P(x)$ is the pressure at that point, η is lubricant viscosity (Pa·s), U is the relative sliding speed of the surfaces (m/s), and ω is the angular speed of oscillation (s^{-1}).

The challenge then is to solve the above equation, subject to appropriate pressure boundary conditions and the load-balance constraint, to find the unknown values ($dh/d\theta$ and x_2) for each value of θ, as θ varies from 0° to 360° for the full reciprocating contact.

Examination of Eq. (4) suggests that the "wedge term" (the first term on the right-hand side of Eq. (4)) will depend on the parameter ηU, as discussed earlier, whereas in contrast, the "squeeze term" (the second term on the right-hand side of Eq. (4)) will depend just on $\eta\omega$.

A detailed analysis finds that there are two non-linear equations that require solving. In the case where "squeeze" effects are neglected, the relevant two equations are:

$$P_2 = P_1 + 6\eta U \int_{-b/2}^{x_2} \frac{ds}{h(s)^2} + 12\eta C_1 \int_{-b/2}^{x_2} \frac{ds}{h(s)^3}, \tag{5}$$

$$\int_{-b/2}^{x_2} P(x) \cdot dx + P_2 \left(\frac{b}{2} - x_2 \right) = P_{back} \cdot b, \tag{6}$$

with:

$$C_1 = -\frac{Uh(x_2)}{2}. \tag{7}$$

When "squeeze" effects are accounted for, the relevant equations are:

$$P_2 = P_1 + 6\eta U \int_{-b/2}^{x_2} \frac{ds}{h(s)^2} + 12\eta C_1 \int_{-b/2}^{x_2} \frac{ds}{h(s)^3} + 12\eta\omega \frac{dh}{d\theta} \int_{-b/2}^{x_2} \frac{s \cdot ds}{h(s)^3}, \tag{8}$$

$$\int_{-b/2}^{x_2} P(x) \cdot dx + P_2 \left(\frac{b}{2} - x_2 \right) = P_{back} \cdot b, \tag{9}$$

where the constant of integration, C_1, which appears in Eq. (8), is given by

$$C_1 = -\frac{Uh(x_2)}{2} - x_2 \omega \frac{dh}{d\theta}. \tag{10}$$

When "squeeze" effects are neglected, the two unknowns that need to be solved for are h_{min} and x_2. However, when "squeeze" effects are included, the two unknowns that are to be solved for are $dh/d\theta$ and the outlet position, x_2.

A complication that can arise when "squeeze" effects are included is that around the reversal positions, it is possible that the oil film covers the entire surface of the slider [17,19], so that $x_1 = -b/2$ and $x_2 = +b/2$. When this occurs, there is just one unknown, $dh/d\theta$, and in this case, only Eq. (9) requires solving, and in addition, for this case, C_1 is given by the equation below:

$$C_1 = \frac{P_2 - P_1 - 6\eta U \int_{-b/2}^{b/2} \frac{ds}{h(s)^2} - 12\eta\omega \frac{dh}{d\theta} \int_{-b/2}^{b/2} \frac{s \cdot ds}{h(s)^3}}{12\eta \int_{-b/2}^{b/2} \frac{ds}{h(s)^3}}. \tag{11}$$

If the minimum OFT at angle θ is h_{min}, then the minimum OFT at angle $(\theta + \Delta\theta)$ can be calculated from:

$$h_{min,i+1} = h_{min,i} + \left(\frac{dh}{d\theta} \right)_i \Delta\theta. \tag{12}$$

The two non-linear equations are solved using Python's fsolve function. The Python function fsolve is a wrapper for the hybrid Powell root-finding method that has been implemented in the FORTRAN 90 library MINPACK [36]. The algorithm can be sped up greatly if the values for $dh/d\theta$ and x_2 from the previous step are used as inputs to the fsolve function at the next step. In addition, the various integrals that appear in Eq. (5) can be evaluated analytically (see Appendix A in Supplementary information), which speeds up the calculations considerably.

For the "squeeze" simulations that are reported later, the Python program typically takes less than 10 s to solve two cycles (720°) at 0.1° intervals (a total of 7,210 points) on a standard desktop computer (such as a Windows 11 Desktop computer with 16 GB of random access memory (RAM) and an Advanced Micro Devices (AMD) Ryzen 5600X 6-core processor).

If, for any reason, there are convergence problems with the numerical solver, these can usually be resolved by repeating the simulation with a lower value for $\Delta\theta$, and simulations have been performed with $\Delta\theta$ as low as 0.01°, although this results in run-times of the order of 100–200 s.

3. Result

3.1. Presentation of data

An example set of data is shown in Figure 2, for the case where A = 5 mm, f = 30 Hz, b = 0.5 mm, η = 10 mPa·s, P_1 = 0, P_2 = 0, and P_{back} = 2 bar (1 bar = 10^5 Pa = 0.1 MPa), and the slider radius of curvature (r) is assumed to be 0.026 m. θ is varied from 0° to 720°. For the simulations without "squeeze", the starting angle is −0.5°, and $\Delta\theta$ = 1°. For the simulations that included "squeeze" effects, the starting angle is −0.05° and $\Delta\theta$ = 0.1°.

Often, in the literature, when "squeeze" effects are included, the minimum OFT in such simulations is not plotted against θ, but rather is plotted against position, or against angle (but the angle is restricted to lie between −90° and +90°). In this case, the same data as from Figure 2 is replotted against position (Figure 3), and it is seen that the minimum OFT differs when the slider moves in different directions. However, plotting the data in such a way complicates the situation, in our view, for non-experts, and for most of the remainder of the paper, data will be plotted in the same way as that in Figure 2, which makes clear

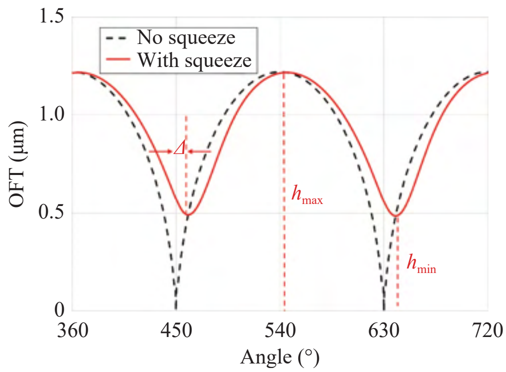

Figure 2 Calculated OFT versus angle. Operating conditions are given in the text. The simulation that includes "squeeze" effects is shown as the red full line, whereas the simulation that neglects such effects is shown as the black dotted line.

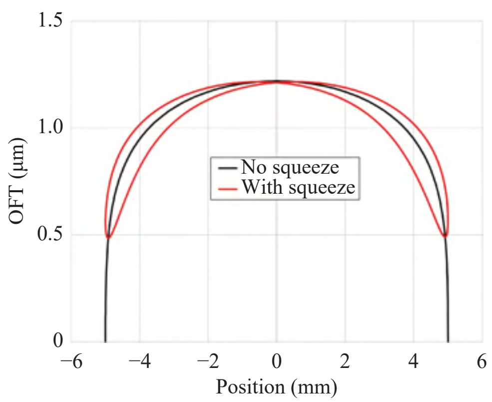

Figure 3 This figure shows the same calculated data as in Figure 2, but this time the OFT data is plotted against position, rather than angle.

how simple the impact of "squeeze" effects is, namely that the minimum OFT occurs at an angle slightly greater than that of the nearest reversal position, and that this minimum value is not zero.

3.2. Maximum oil film thickness data

The maximum OFT, h_{max}, is not expected to be impacted significantly by the inclusion of "squeeze" effects, and so useful insight into the variation of h_{max} with the key variables (A, f, b, η, P_{back}, and r) can be obtained using the Python program that does not include "squeeze" effects.

A useful dimensionless variable, S, can be defined as

$$S = \frac{\eta \omega A}{P_{back} b}. \tag{13}$$

Numerous simulations have been performed, in which the various parameters (A, f, b, η, P_{back}, and r) are varied over a wide range, and this data is available in the Supplementary Data file of the Supplementary information.

As has been reported by other researchers [11,13,17], it has been found, from the numerical simulations, that the maximum OFT varies with the slider radius of curvature, and that there is an optimum radius of curvature, r_o, at which the maximum OFT has its highest possible value (for a given set of A, f, b, η, and P_{back}).

When r_o / b was plotted against S on a log-log scale, it was found that the data points from all the numerous simulations lay on a straight line, suggesting that there was a power law relationship between r_o/b and S. Excel's Solver function was used to find the best fit equation for this power law, and the resulting expression was found to be:

$$\frac{r_o}{b} = \frac{0.405}{\sqrt{S}}. \tag{14}$$

In addition, it was found that when $h_{max}(r)/h_{max}(r_o)$ was plotted against r/r_o (on a logarithmic scale), all the data lay on a common curve (Figure 4). The actual data points on which this figure is based are available as Supplementary Data to this paper.

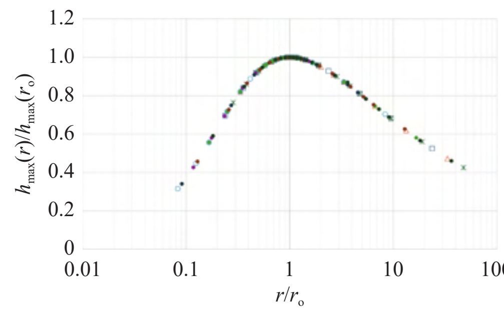

Figure 4 Graph showing how $h_{max}(r)/h_{max}(r_o)$ varies with r/r_o. The coloured dots are the results of the many numerical simulations in which A, b, η, f, and P_{back} were varied.

If the curve shown in Figure 4 is defined to be $C_{max}(r/r_o)$, then the value of $h_{max}(r)$ can be related to $h_{max}(r_o)$ by

$$h_{max}(r) = C_{max}\left(\frac{r}{r_o}\right) h_{max}(r_o). \tag{15}$$

When the value of $h_{max}(r_o)/b$ was plotted against S, on a log-log scale, it was also found that the data points lay on a straight line, suggesting that a power law type relationship relates $h_{max}(r_o)/b$ to S. Once again, Excel's Solver function was used to find the best fit power law equation to the data, which was:

$$\frac{h_{max}(r_o)}{b} = 0.2524\sqrt{S}. \tag{16}$$

Therefore, using Eqs. (15) and (16), it is found that:

$$\frac{h_{max}(r)}{b} = 0.2524 C_{max}\left(\frac{r}{r_o}\right)\sqrt{S}. \tag{17}$$

Equation (17) is for the maximum OFT, which occurs at angles of 0°, 180°, 360°, etc. For a general angle θ, when "squeeze" films are ignored, the OFT, $h(\theta)$, in the contact can be well approximated as

$$\frac{h(\theta)}{b} = 0.2524 C_{max}\left(\frac{r}{r_o}\right)\sqrt{S|\cos\theta|}. \tag{18}$$

In addition, by fitting a suitable curve to the data shown in Figure 4, an approximate analytical expression for $C_{max}(r/r_o)$ was found and is given below:

$$C_{max}\left(\frac{r}{r_o}\right) = 1 - A\log_{10}\left(\frac{r}{r_o}\right) - B\left[\log_{10}\left(\frac{r}{r_o}\right)\right]^2. \tag{19}$$

For $r/r_o < 1$, $A = 0$, and $B \approx 0.657$, whilst for $r/r_o > 1$, $A \approx 0.092$, and $B \approx 0.186$. Equation (19) provides a reasonable fit to the data shown in Figure 4. This fit is valid for r/r_o in the range 0.1 to 50.

Table 1 gives the values of $C_{max}(r/r_o)$ for values of r/r_o varying from 1/10 to 10. Intermediate values can be interpolated

Table 1 Calculated values of $C_{max}(r/r_o)$ for r/r_o varying from 1/10 to 10

r/r_o	$C_{max}(r/r_o)$	r/r_o	$C_{max}(r/r_o)$
1/10	0.366	3/2	0.983
1/9	0.401	2	0.952
1/8	0.442	3	0.893
1/7	0.491	4	0.843
1/6	0.551	5	0.802
1/5	0.623	6	0.768
1/4	0.712	7	0.740
1/3	0.816	8	0.714
1/2	0.927	9	0.693
3/4	0.987	10	0.673
1	1	–	–

from the data in Table 1.

Equation (17) is a significant improvement over previously reported approximations [6,7], since it explicitly includes the impact of the slider radius of curvature. In addition, it is believed that it is the first time that an equation has been proposed to predict the optimum radius of curvature for a parabolic sliding line contact (Eq. (14)).

As a specific example, consider the case where A = 5 mm, η = 10 mPa·s, f = 20 Hz, P_{back} = 2 bar, where the slider width, b, is varied from 0.25 mm to 1.5 mm. Table 2 shows the calculated value of r_o (which is the slider radius of curvature, which will give the highest film thickness at mid-stroke) and also the value of Δh (the inlet height, which is equal to $b^2/8r$, for a symmetric parabolic contact). Δh is simply the difference in height between the center and edge of the parabolic slider.

Table 2 Calculated values of r_o and Δh, for different slider widths, b (operating conditions given in the text)

Slider width/mm	r_o/m (Eq. (14))	$\Delta h = b^2/(8r_o)$/μm
0.25	0.009,0	0.87
0.5	0.025,6	1.22
0.75	0.046,9	1.50
1.0	0.072,3	1.73
1.25	0.101,0	1.93
1.5	0.132,8	2.12

The optimum radius of curvature, as shown in Table 1, seems to correspond to an inlet height, Δh, of between approximately 1 and 2 micrometers, for these specific operating conditions.

It should be emphasized, however, that the variation of maximum OFT with slider radius of curvature is quite a slowly varying function. Even if $1/3 \leqslant r/r_o \leqslant 3$, the maximum OFT, $h_{max}(r)$, is still greater than about 82% of $h_{max}(r_o)$.

Figure 5 shows a comparison of numerical calculations of OFT versus crank angle, compared to the simple Eq. (18), where the numerical simulations were evaluated at 1° intervals, whereas Eq. (18) was applied at 15° intervals. The operating conditions for this comparison were: A = 40 mm, b = 1,000 μm, f = 50 Hz, η = 5 mPa·s, and P_{back} = 5 bar, for r = 0.005, 0.036, and 0.2 m.

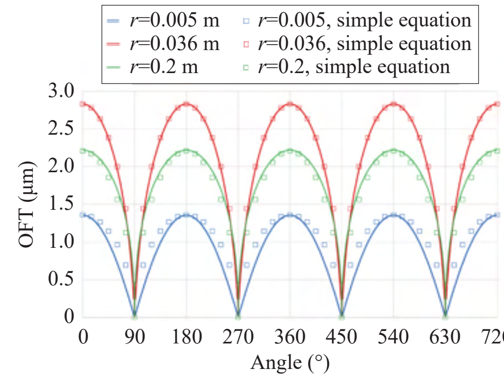

Figure 5 Comparison of the use of the simple equation (Eq. (18)) for estimation of OFT in reciprocating contact, compared to a full numerical simulation, for different slider radii of curvature.

3.3. Minimum oil film thickness data

When "squeeze" effects are included, the minimum OFT in the contact is no longer zero, and the position of the minimum is shifted to a slightly greater angle compared to the closest reversal position. For example, for the data shown in Figure 2, the minimum OFT is calculated (numerically) to be 0.485 μm, and the position of the minimum is shifted to a position such as $(90 + \Delta)°$, or $(270 + \Delta)°$, where $\Delta \approx 10.3°$.

Experimental data [25–27] are available which suggest that the minimum OFT increases with (1) viscosity, η, and (2) angular speed, ω, while it decreases with (3) load. Data have also been reported that suggest that the minimum OFT increases as the slider radius of curvature increases (i.e., as the slider becomes "flatter") [17]. It is not clear how the amplitude of oscillation, A, and the slider width, b, impact the minimum OFT.

Many simulations have been performed using the Python software (described in Sect. 3) that models hydrodynamic reciprocating lubrication, which includes the "squeeze film" effect, and this data has been used to find approximate formulae for h_{min} (and its variation with contact radius of curvature) and the position, Δ, at which the minimum OFT position occurs.

It was reported in Sect. 3.2 that the maximum OFT varied with the slider radius of curvature (as shown in Figure 4). Detailed simulations have found that the minimum OFT is also sensitive to the slider radius of curvature. An example of this is shown in Figure 6 below (for which the following values were used in the simulation: A = 5 mm, b = 0.5 mm, η = 10.0 mPa·s, P_{back} = 2 bar, and f = 20 Hz). As expected, the maximum OFT predicted by the model that includes "squeeze" effects is essentially the same as that for the model that neglects "squeeze" effects, and this is because "squeeze" effects are not significant at the mid-stroke positions of reciprocating contacts. It is also observed that there is an optimum radius of curvature at which the minimum OFT achieves its highest value, but that this optimum radius is significantly larger than the radius of curvature that leads to the highest maximum OFT. For the example shown in Figure 6, the radius of curvature that gives the highest film thickness at mid-stroke is approximately 0.025,5 m (corresponding to a Δh of about 1.2 μm), whilst the radius of curvature that gives the highest minimum OFT is approximately 0.1 m (corresponding to a Δh of only about 0.3 μm).

Similar results to those shown in Figure 6 have been previously reported by Economou [13].

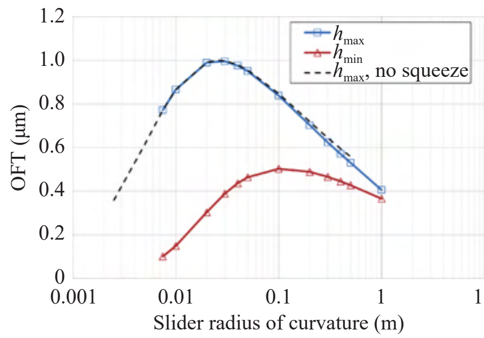

Figure 6 Variation of h_{min} and h_{max} for "squeeze" simulations. Data from simulations without "squeeze" effects are also shown for h_{max} (black dashed line).

Denote the optimum radius of curvature for h_{min} by r_{sq}. If the detailed variation of r_{sq}/b is to take a similar form to that found for r_o/b (Eq. (14)), it has been found useful to introduce the dimensionless parameter S_Q, where S_Q is defined to be:

$$S_Q = \frac{\eta\omega}{P_{back}}\sqrt{\frac{A}{b}}. \tag{20}$$

From a detailed analysis of the data from the set of numerical simulations (which can be found in the Supplementary Data of the Supplementary information), it was found that when r_{sq}/b was plotted against S_Q, on a log-log scale, the various data points lay on a straight line, suggesting a power law relationship between r_{sq}/b and S_Q, and the best fit power law equation was found to be:

$$\frac{r_{sq}}{b} \approx \frac{0.82}{\sqrt{S_Q}}. \tag{21}$$

A graph can be plotted of $h_{min}(r)/h_{min}(r_{sq})$ versus r/r_{sq}, in a similar way to that carried out for the maximum OFT (Figure 4), and it has been found that data from many simulations, in which S_Q is varied, fit onto a common curve, as shown in Figure 7.

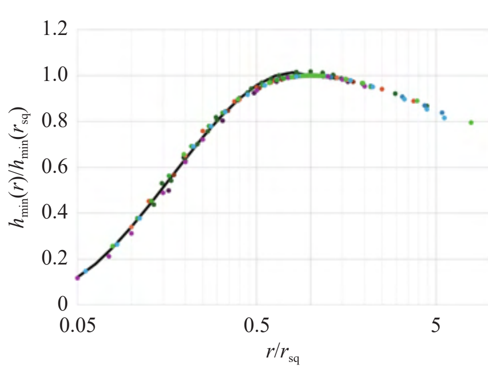

Figure 7 Graph showing $h_{min}(r)/h_{min}(r_{sq})$ versus r/r_{sq} for many different sets of operating conditions. The resulting curve is defined to be $C_{min}(r/r_{sq})$. The black line shows a third-order polynomial fit (in powers of $\log_{10}(r/r_{sq})$) to the data for $0.05 \leqslant r/r_{sq} \leqslant 1$.

A third-order polynomial fit to the data (Figure 7) provides a reasonable fit, and the equation for this is:

$$C_{min}\left(\frac{r}{r_{sq}}\right) \approx 1 - B_1\log_{10}\left(\frac{r}{r_{sq}}\right) - B_2\left[\log_{10}\left(\frac{r}{r_{sq}}\right)\right]^2 - B_3\left[\log_{10}\left(\frac{r}{r_{sq}}\right)\right]^3. \tag{22}$$

When the range is $0.05 \leqslant r/r_{sq} \leqslant 1$, the best fit to the data in Figure 7 was found for: $B_1 = 0.29$, $B_2 = 1.64$, and $B_3 = 0.69$.

From Figure 7, it follows that:

$$h_{min}(r) = C_{min}\left(\frac{r}{r_{sq}}\right) h_{min}(r_{sq}). \tag{23}$$

Analysis of the data points from many numerical simulations in which A, b, η, ω ($\omega = 2\pi f$), and P_{back} have been varied has found that when $h_{min}(r_{sq})/b$ was plotted against S_Q, on a log-log scale, the data points lay on a straight line, so that a power law relationship relates $h_{min}(r_{sq})/b$ to S_Q. The best fit power law equation was found to be:

$$\frac{h_{min}(r_{sq})}{b} = 0.22\sqrt{S_Q}. \tag{24}$$

Therefore, a general expression for $h_{min}(r)$ is given by

$$\frac{h_{min}(r)}{b} = 0.22 C_{min}\left(\frac{r}{r_{sq}}\right)\sqrt{S_Q}. \tag{25}$$

Numerical investigations have shown that the angular position at which the minimum film thickness occurs (which will be at positions such as $(90 + \varDelta)°$ and $(270 + \varDelta)°$) depends on the ratio of the minimum and maximum OFT, h_{min}/h_{max}, and also on the ratio A/b. Figure 8 shows how $\varDelta$ (°) varies with h_{min}/h_{max} for different values of A/b.

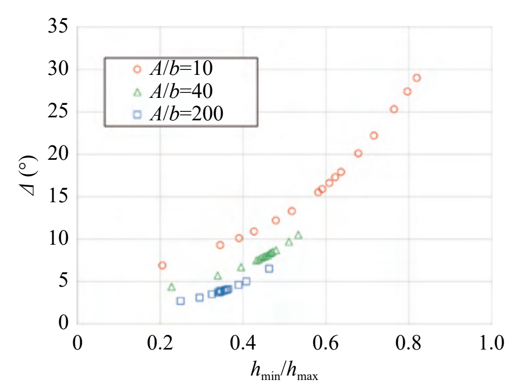

Figure 8 Graph showing how $\varDelta$ (°) varies with h_{min}/h_{max} for different values of A/b.

Figure 9 shows the same data as in Figure 8, but now $\varDelta$ is plotted against $(h_{min}/h_{max})(b/A)^{0.25}$.

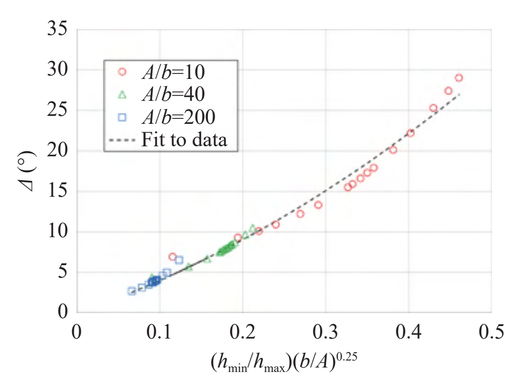

Figure 9 Graph showing how $\varDelta$ (°) varies with $(h_{min}/h_{max})(b/A)^{0.25}$ for different values of A/b. The black dashed line is a fit to the data, as described in the paper.

From Figure 9, a relatively simple expression for $\varDelta$ can be obtained, where, in the equation below, z is defined to be

$(h_{min}/h_{max})(b/A)^{0.25}$:

$$\Delta = A_1 z + A_1 z^2, \quad (26)$$

where the angle Δ is in degrees. A good fit to the data was obtained using A_1 = 35.0 and A_2 = 51.1. This fit is shown as the dotted line in Figure 9.

The astute reader may have realized that $(h_{min}/h_{max})(b/A)^{0.25}$ can be simplified (using Eqs. (17) and (25)) to become:

$$\left(\frac{h_{\min}}{h_{\max}}\right)\left(\frac{b}{A}\right)^{0.25} = \frac{0.22C_{\min}\left(\frac{r}{r_{\text{sq}}}\right)}{0.2524C_{\max}\left(\frac{r}{r_{\text{o}}}\right)}\sqrt{\frac{b}{A}} \approx$$

$$0.87\left[\frac{C_{\min}\left(\frac{r}{r_{\text{sq}}}\right)}{C_{\max}\left(\frac{r}{r_{\text{o}}}\right)}\right]\sqrt{\frac{b}{A}}. \quad (27)$$

At first sight, from Eq. (27), it would appear that Δ just depends on r, A, and b, but in fact, the values of r_o and r_{sq} depend on parameters η, ω, and P_{back} too.

It is also worth noting that h_{min}/h_{max} depends on $(b/A)^{0.25}$. The implication of this result is that this ratio should get larger as the amplitude of oscillation is reduced (provided the slider width is constant).

4. Validation of the model

It is highly desirable to validate numerical models by comparison with experimental data. The models described above (now written in Python) are similar, but substantially modified and improved (for robustness and speed) versions of software originally developed for predicting OFT and friction losses for piston rings. As such, the models gave good agreement with both experimentally measured OFT and friction losses for piston rings [37,38]. However, for the piston ring application, the values of P_1, P_2, P_{back}, and η varied substantially across the cycle, and in addition, the speed variation was not as simple as that described by Eq. (3), since there is a crank slider arrangement (as discussed later).

It is also worth noting that the equation for the maximum OFT (Eq. (17)) is consistent with previously reported equations by Furuhama and Sasaki [6] and McGeehan [7].

Numerous crank angle resolved OFT measurements, in a reciprocating tribometer, have been reported by Dellis [25–27], for different lubricants, operating at different temperatures, loads, and speeds. It was found that over the range of conditions tested, the minimum OFT was in the range 0.3 μm to 0.9 μm. In addition, it was noted that the position of the minimum OFT was shifted to "a few degrees of crank angle after the dead centers" [26].

Taking two specific examples, Figure 10 shows a comparison of model results with experimental data from Dellis [26]. The experimental data contained in the graphs of [26] were digitized, and the digitized data are shown in Figure 10, whereas the model results are shown by the line. For the simulation in Figure 10, the following data were used: A = 25 mm, b = 5 mm, f = 5 Hz, r = 80 mm, η = 55.8 mPa·s, with P_{back} = 1.94 bar (low load) and 5.65 bar (high load). These loads correspond to a load per unit length of 971 and 2,823 N/m, respectively.

For the low load case, the maximum OFT appears to be overestimated by the model. This could be because the model assumes Newtonian lubricants, whereas Oil 7B, the oil used in the experiment, is a viscosity-modified lubricant (with a viscosity

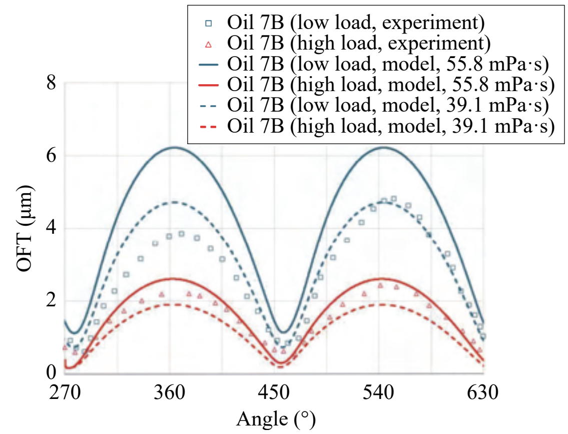

Figure 10 Comparison of OFT experimental data [26] (square and triangle data points) with model (solid or dotted lines) for Oil 7B, at low and high loads (971 and 2,823 N/m, respectively).

grade of SAE 0W-40), and so there will be temporary shear thinning in the contact, which would mean the lubricant viscosity is lower than that assumed in the model. The agreement between the model and the experiment seems better for the high-load case. For an SAE 0W-40 lubricant grade, with the experiments being carried out for a lubricant temperature of 40 °C (and shear rates in the contact being greater than 10^5 s^{-1}), it is likely that the actual lubricant viscosity in the contact is about 30% lower [39] than the predicted Newtonian value (due to temporary shear thinning) and so the numerical simulations were re-done using a viscosity of 39.1 mPa·s. These results are also shown in Figure 10 as dotted lines. It is also worth noting that the fact that the maximum OFT is different during the cycle, for the experimental data, is likely due to experimental artefacts (Dellis [26] stated that as the load is only applied at one end of the stroke, it is thought the load is not constant throughout the cycle, and so it is likely that at one maximum, the load is lower than the average value, whilst at the other maximum it is higher—clearly these effects are not included in the model predictions).

Separately, Dellis [26] also looked at the impact of temperature on OFT. As an example, Figure 11 shows experimental data points for Oil 5A for temperatures of 33, 50, and 68 °C in comparison with model predictions (shown by the solid or dotted lines). Oil 5A is an SAE 0W-20 lubricant viscosity grade (with V_k40 =

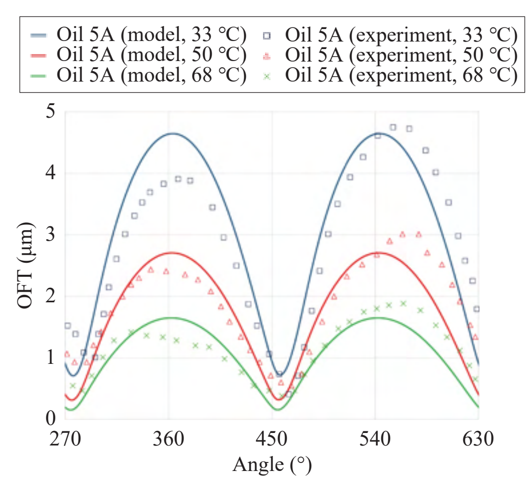

Figure 11 Comparison of OFT experimental data [26] (squares, triangles, and crosses data) with model (solid or dotted lines) for Oil 5A, for oil temperatures of 33, 50, and 68 °C.

31 mm^2/s and V_k100 = 6.04 mm^2/s). At the measured oil temperatures (33, 50, and 68 °C), the calculated oil dynamic viscosities are estimated to be 34.4, 18.0, and 10.3 mPa·s, respectively. As this oil is an SAE 0W-20 grade, it is not expected to exhibit as much temporary shear thinning as the 0W-40 grade considered in Figure 10, and so such effects have not been considered here.

Therefore, for these simulations, A = 25 mm, b = 5 mm, f = 6.67 Hz, r = 80 mm, P_{back} = 2.32 bar, and viscosities, η, of 34.4, 18.0, and 10.3 mPa·s, respectively, were used.

Separately, Bolander et al. [40] have independently reported friction measurements in a reciprocating test rig (in which A = 33.35 mm) designed to simulate piston ring lubrication. From the measured friction coefficient measurements, the OFT variation throughout the contact cycle was inferred, and the variation of OFT throughout the contact for different oscillation frequencies was reported, as was the impact of load on the OFT.

For that test rig [40], for the experiments in which the load was kept constant and the oscillation frequency varied, the relevant parameters are: A = 33.35 mm, b = 3.79 mm, r = 34.5 mm, P_{back} = 430 bar, η = 200 mPa·s, and f = 2, 3, and 5 Hz. The OFT results reported by Bolander et al. [40] have been digitized and shown below in Figure 12 as separate data points, where they are compared with predictions of the model from this paper (shown as lines in Figure 12).

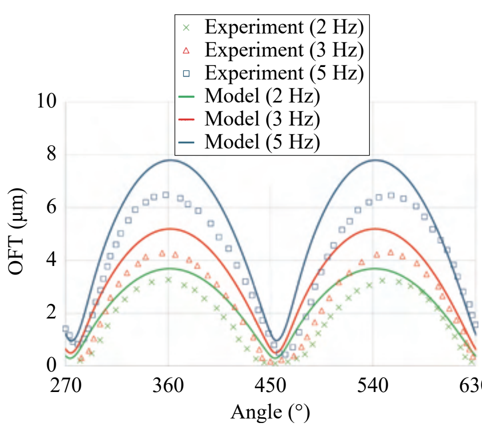

Figure 12 Comparison of model predictions (solid lines) with OFT data published by Bolander et al. [40], showing the impact of different frequencies.

The model seems to overestimate the maximum OFT compared to the results reported by Bolander et al. [40]. However, the model does assume fully flooded lubrication, and in their particular experiment [40], the contact was not run in an oil bath, but rather "two rows of 15 drops of SAE 30 oil (1.0 mL) were evenly distributed over the entire stroke of the liner segment", so there may not be enough oil to flood the contact at mid-stroke fully. In addition, no account is taken of possible shear heating of the lubricant (if this did occur, the viscosity of the lubricant would be lower than assumed in the model calculations).

Overall, the agreement between the model and the results reported by Dellis [25–27] and Bolander et al. [40] is considered reasonable and helps to validate the model reported here.

5. Application

5.1. General equation for OFT versus angle—with "squeeze" effects included

If the maximum OFT (found from Eq. (17)) is h_{max}, the minimum OFT (found from Eq. (25)) is h_{min}, and the angular position at which the minimum occurs (found from Eq. (26)) is Δ (°), then a simple equation that could be used to predict the OFT for any angle, θ, should take the form below:

$$h(\theta) = h_{min} + (h_{max} - h_{min})\,|\cos(\theta - \Delta)|. \tag{28}$$

Figure 13 shows the results for two numerical simulations with widely different A/b ratios. Simulation #1 has: A = 50 mm, b = 0.5 mm, η = 10 mPa·s, f = 30 Hz, r = 0.01 m and P_{back} = 2 bar, whereas Simulation #2 has: A = 5 mm, b = 1 mm, η = 10 mPa·s, f = 30 Hz, r = 0.1 m and P_{back} = 2 bar.

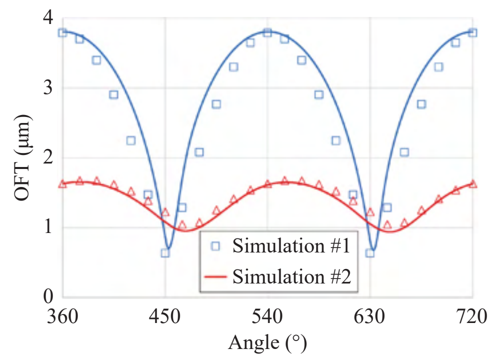

Figure 13 Comparison of simple equation for OFT variation with angle (Eq. (28)) shown as blue squares and red triangles, with full numerical simulations, using Python code (blue and red lines).

Separately, for the two simulations, the values of h_{min}, h_{max}, and Δ have been estimated using Eqs. (17), (25), and (26). The calculations also required the parameters r_o and r_{sq} to be evaluated, using Eqs. (14) and (21).

For Simulation #1, the simple equations are used to find that: h_{min} = 0.54 μm, h_{max} = 3.79 μm, and Δ = 1.7°. (In this calculation, r_o, r_{sq}, $C_{min}(r/r_{sq})$, and $C_{max}(r/r_o)$ were also calculated, with values of: r_o = 0.006,6 m, r_{sq} = 0.042,2, $C_{max}(r/r_o)$ = 0.977, and $C_{min}(r/r_{sq})$ = 0.708. These values were calculated using Eqs. (14), (19), (21), and (22)).

For Simulation #2, the simple equations are used to find that: h_{min} = 0.97 μm, h_{max} = 1.68 μm, and Δ = 21.2°. (In addition, it was found that: r_o = 0.059 m, r_{sq} = 0.179, $C_{max}(r/r_o)$ = 0.969, and $C_{min}(r/r_{sq})$ = 0.980.)

5.2. Application to wear

Figure 14 shows a typical schematic cross-section of the type of wear scar found in reciprocating tribometers [41]. If y is the distance between the maximum wear depth and the edge of

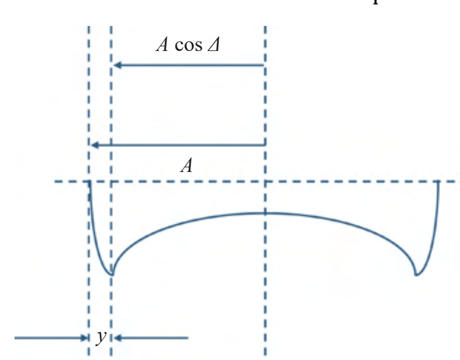

Figure 14 Schematic of wear profile found in reciprocating wear tests [41].

the contact, then:

$$\frac{y}{A} = 1 - \cos\Delta. \tag{29}$$

The angle Δ can be estimated from a measurement of y, and once Δ is known, h_{min}/h_{max} can be estimated from Eq. (26), and since h_{max} can be readily calculated (from Eq. (17)), values of both h_{min} and h_{max} can be found. Since the values of h_{min}, h_{max}, and Δ are available, the OFT throughout the contact cycle can be estimated using Eq. (28). Note that this analysis assumes low contact pressures so that hydrodynamic lubrication conditions apply, although it could be envisaged that a similar type of calculation could be performed for elastohydrodynamic contacts too.

5.3. Comparison of OFT estimates for piston rings

There have been many published papers on OFT estimates for piston rings [9–20]. The piston ring problem is slightly more complex than the one solved here, because (1) the load on the back of the ring varies over the reciprocating cycle (due to changing combustion pressures), (2) the viscosity also varies over the cycle since there is a temperature gradient along the liner, with temperatures at BDC being lower than those at TDC, and (3) the position and speed of the piston ring are not as simple as those described by Eqs. (1) and (3). There is a crank-slider mechanism, in which the rotational motion of the crankshaft is converted to linear motion of the piston via the con-rod. The speed of the piston ring relative to the liner is given by an equation of the form below:

$$U = \omega R\left[\sin\theta + \left(\frac{R}{2L}\right)\frac{\sin 2\theta}{\sqrt{1-\left(\frac{R}{L}\right)^2\sin^2\theta}}\right], \tag{30}$$

where U is the speed (m/s) of the piston ring relative to the liner, ω is the angular speed (rad/s), R is the crank radius (m), and L is the con-rod length (m).

Notwithstanding this more complex motion, to a first approximation it can be considered as a simple reciprocating contact (since the con-rod length is usually much larger than the crank radius), with the amplitude of oscillation being equal to the crank radius, R (which is half the engine's stroke).

Recently published data [15] modeled a fully flooded top piston ring, which included "squeeze" effects, and the following values were reported: St = 78.7 mm (St is the engine stroke (mm)), so R = 39.35 mm (and con-rod length L is 154 mm), b = 1.5 mm, r = 0.1 m, P_{back} = 1.71 bar, N = 2,500 r/min (N is the engine speed (revs per minute)), so ω = 261.8 rad/s (corresponding to a frequency f of about 41.67 Hz). The value of R is effectively the amplitude A, as defined in this paper. The value of P_{back} used for BDC and mid-stroke calculations is effectively just due to the piston ring tension (as pressures in the ring-pack will be close to atmospheric at these positions). BDC liner temperature was 100 °C, and TDC liner temperature was 150 °C, so the lubricant viscosity at BDC would be roughly 10 mPa·s, and that at TDC would be about 3.5 mPa·s (and at mid-stroke it could be assumed that the viscosity would be about 6 mPa·s). The load on the piston ring at TDC firing will be much higher than at BDC, due to the increased combustion chamber pressure acting on the back of the piston ring (which is in addition to the ring tension). A reasonable value to use for P_{back} at TDC would be 20 bar. Using this data, we can estimate the OFT at mid-stroke (from Eq. (17)) and the minimum OFT at BDC and at TDC firing (from Eq. (25)).

Estimates are obtained as follows: mid-stroke OFT ≈ 5.48 μm, minimum OFT at BDC ≈ 2.98 μm, and minimum OFT at TDC firing ≈ 0.094 μm. These numbers are in reasonable agreement with the data published in Ref. [15] despite the fact that there are uncertainties as to the correct value of P_{back} to use at TDC.

Data from Ref. [15] lists the minimum OFT at TDC firing, at 1,000 r/min, for different values of r. Table 4 lists the reported values [15] together with estimated values (from Eq. (21)). For these simulations, P_{back} has been reduced to 10 bar, since it is unlikely that the engine will be at full load for a speed of 1,000 r/min.

Table 4 Comparison of reported OFT values at TDC firing versus radius of curvature from Ref. [15] and predictions from Eq. (25)

Piston ring radius of curvature/m	OFT at TDC firing (Ref. [15])/μm	OFT at TDC firing (Eq. (25))/μm
0.05	0.068	0.01
0.10	0.19	0.07
0.20	0.37	0.21
0.40	0.51	0.39

The results from the simple equation described above are directionally similar but the simple model consistently underpredicts the minimum OFT, although it must be emphasized that there are some uncertainties in the pressure acting on the back of the piston ring, the exact viscosity to use, and the position and speed variation of the piston ring is more complex than the simple sinusoidal functions used in Eqs. (1) and (3).

6. Discussion

6.1. Effect of slider radius of curvature on lubrication regime and wear

In many cases, it is found that the slider radius of curvature is optimized to maximize the mid-stroke OFT. When this is done, the slider radius of curvature will typically be much lower than the optimum value that maximizes the minimum OFT. This will likely result in lubrication conditions close to reversal positions being in the mixed or boundary regimes. Wear would then be expected to occur in the vicinity of the minimum OFT position. If the slider is softer than the flat surface it is sliding against, this wear would be expected to result in a "flattening" of the curved slider over time, so that the slider radius of curvature increases, which will then lead (according to the theory outlined above) to a higher OFT around the reversal positions. In fact, Priest et al. [42] have reported experimental data on piston rings during the "running-in" period in which this exact mechanism was observed.

On the other hand, if the slider is harder than the flat surface, then wear would be expected to occur mainly on the flat surface, rather than the slider. The highest amount of wear would occur at the position where the minimum OFT is expected to occur (slightly inbound of the reversal position). Then the combined radius of curvature would become a function of position, with a higher radius of curvature occurring closer to reversal positions (favoring higher OFT due to squeeze effects), whereas the radius of curvature would be unchanged around mid-stroke positions. From a tribological point of view, it would seem preferable to have a slider of higher hardness. It also suggests that the work reported here should be extended, in the future, to allow for the possibility of a position-dependent radius of curvature.

It is also worth considering whether a higher radius of curvature should be chosen for the slider in the first place. This would result in a lower mid-stroke OFT (although at mid-stroke the film thickness is relatively thick anyway) but would result in a higher minimum OFT, which would mean there would be less mixed/boundary lubrication (and less wear) compared with choosing a slider whose radius of curvature is optimized for mid-stroke film thickness. If the slider radius of curvature is too small, however, it is likely, during the "running-in" process, that wear will occur, which will naturally result in the effective radius of curvature increasing anyhow. To give a specific example, consider a simulation in which A = 10 mm, b = 1.5 mm, f = 20 Hz, η = 5 mPa·s, and P_{back} = 5 bar, for different slider curvature radii. Table 5 shows the calculated values of h_{min}, h_{max}, and Δ for different values of r.

Table 5 Results showing how the minimum OFT can be increased by increasing the slider radius of curvature

Slider radius of curvature/m	h_{min}/μm	h_{max}/μm	h_{min}/h_{max}	Δ/(°)
0.05	0.03	1.080	0.028	0.6
0.1	0.149	1.107	0.135	3.3
0.2	0.374	1.098	0.340	9.7
0.5	0.607	1.029	0.590	19.7
1.0	0.486	0.934	0.520	16.7

6.2. Asymmetry of OFT with slider direction of travel

It has been noted by numerous researchers that the OFT and friction, in reciprocating tribometers, with symmetric sliders, are not symmetric. The OFT (and friction) is different when the slider is moving to the left compared to when the slider is moving to the right. This effect has been attributed to the squeeze effect. As has been discussed above, a key parameter related to the squeeze effect is the parameter Δ. If there are no squeeze film effects, Δ = 0, h_{min} would also be zero, and the OFT would be the same in either direction. As Δ increases, the asymmetrical effects become more pronounced. As an illustration of this, the data in Figure 13 has been replotted in Figure 15, versus position (rather than angle). For the data in Figure 15, Simulation #1 had: A = 50 mm, b = 0.5 mm, η = 10 mPa·s, f = 30 Hz, r = 0.01 m, and P_{back} = 2 bar; and Simulation #2 had: A = 5 mm, b = 1 mm, η = 10 mPa·s, f = 30 Hz, r = 0.1 m, and P_{back} = 2 bar.

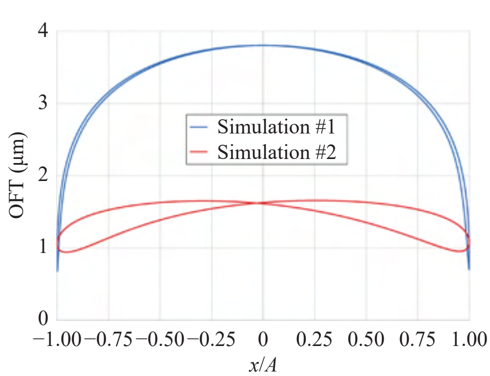

Figure 15 Replot of data from Figure 13, showing OFT data versus position (normalized to the amplitude of oscillation).

Figure 16 also shows detailed data of calculated OFT versus position (from the simulations reported in Table 5), showing how the asymmetry is also impacted by the slider radius of curvature if the amplitude is fixed. For the simulations in Figure 16, details were: A = 10 mm, b = 1.5 mm, η = 5 mPa·s, f = 20 Hz, and P_{back} = 5 bar.

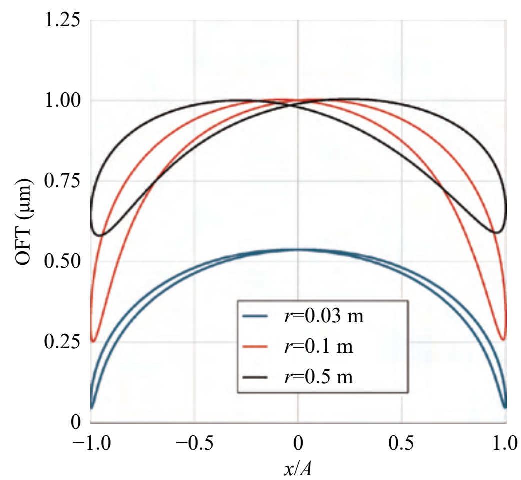

Figure 16 Graph showing how the asymmetry in OFT is influenced by the slider radius of curvature, for fixed amplitude.

6.3. Impact of the A/b ratio

An intriguing finding from this work is that the ratio of the minimum to maximum OFT is influenced greatly by the parameter A/b. For large values of this ratio, h_{min}/h_{max} will be small. As an example, in Figure 13, when A/b = 100, h_{min}/h_{max} is approximately 0.2; whereas when A/b = 5, h_{min}/h_{max} is approximately 0.57.

6.4. Novel aspects of this work

For the first time, simple analytical equations are as shown below.

(1) The value of the minimum OFT in a hydrodynamic reciprocating line contact.

(2) The angular position (Δ) by which the minimum OFT is displaced from the reversal position.

(3) The optimum slider radius of curvature (r_o) that maximizes the mid-stroke OFT.

(4) The optimum slider radius of curvature (r_{sq}) that maximizes the minimum OFT (close to reversal positions)—this is usually a few times higher than r_o.

(5) Rather than perform simulations in which key parameters (such as the amplitude and slider width) are fixed, as is normally reported in the literature in both experimental and modeling work, simulations have been performed for a much wider range of key parameters (A, b, η, f, P_{back}, r) than those usually considered.

In addition, a greatly improved equation has been reported for the maximum OFT, which clarifies how this value varies with the slider radius of curvature.

The model has been tested against a small number of good-quality experimental measurements of OFT in reciprocating contacts, and reasonable agreement has been found.

One novel, and perhaps surprising, finding of the work reported here is that the parameter (A/b) is important for determining the value of Δ (which is a key parameter for estimating how asymmetric the OFT variation across the contact is) and also in determining the ratio h_{min}/h_{max}. The results reported here suggest that the OFT asymmetry would be most pronounced for contacts that have a low (A/b) value and in which the slider radius of curvature is high (i.e., the slider contact is flatter).

7. Conclusion

Equations have been derived for the maximum OFT, h_{max}, the minimum OFT, h_{min}, and its angular position, Δ, for a reciprocating hydrodynamic contact. These are:

$$h_{max} = C_{max}\left(\frac{r}{r_o}\right)H_{max}, \tag{31}$$

$$h_{min} = C_{min}\left(\frac{r}{r_{sq}}\right)H_{min}, \tag{32}$$

$$\Delta \approx 35.0\left(\frac{h_{min}}{h_{max}}\right)\left(\frac{b}{A}\right)^{0.25} + 51.1\left(\frac{h_{min}}{h_{max}}\right)^{2}\left(\frac{b}{A}\right)^{0.5}, \tag{33}$$

where H_{max} and H_{min} are given by

$$\frac{H_{max}}{b} = 0.2524\sqrt{\frac{\eta\omega A}{P_{back}b}}, \tag{34}$$

$$\frac{H_{min}}{b} = 0.22\left(\frac{A}{b}\right)^{0.25}\sqrt{\frac{\eta\omega}{P_{back}}}. \tag{35}$$

Using the parameters h_{min}, h_{max}, and Δ, the full OFT versus angle curve, for a hydrodynamic reciprocating contact, can be estimated (using Eq. (28)) without the need for a numerical solution of the Reynolds' equation.

The results presented here should be of interest to users (and manufacturers) of reciprocating tribology test machines, and it has also been shown that reasonable estimates of piston ring OFT can be obtained for mid-stroke, BDC, and TDC positions, despite the parameters for the piston ring problem being quite different compared to the data sets that the above equations were derived from.

There was also a brief discussion of the possibility of estimating the position, Δ, of the minimum OFT by careful measurement of wear scars in reciprocating test rigs. This position can then be used to estimate the ratio, h_{min}/h_{max}, and since h_{max} can readily be determined from the operating conditions of the test rig, all three parameters could be estimated from experimental wear data in reciprocating test rigs, and the OFT versus angle variation that was present in the test could be reconstructed.

Clearly, the results presented here assume hydrodynamic lubrication. It would be instructive to repeat the calculations reported here for elastohydrodynamic lubrication conditions, although it would be expected that OFT will be larger under elastohydrodynamic conditions (at least if isothermal conditions are assumed), so the calculations reported here provide a useful engineering lower limit on OFT values. It is the intention of future research to apply the methods reported here to reciprocating contacts in the elastohydrodynamic regime.

In addition, an intriguing relationship has been found between the ratio of the minimum to maximum OFT, h_{min}/h_{max}, and the ratio, A/b, where A is the amplitude of oscillation and b is the slider width.

This paper is the first attempt to provide improved clarity regarding issues surrounding squeeze film lubrication in reciprocating sliding contacts. Future work is planned to improve the model by (1) including the effect of surface roughness, (2) extending the analysis to include the elastohydrodynamic regime, (3) extending the analysis to allow for elliptical (and point) contacts, and (4) including more complex fluid rheology to allow for lubricants such as grease.

Supplementary information

The supporting information is available online at https://doi.org/10.3724/trad-20260006. The supporting materials are published as submitted, without typesetting or editing. The responsibility for scientific accuracy and content remains entirely with the authors.

Conflict of interests

The author(s) declare that they have no conflict of interest.

Acknowledgements

The author would like to thank his colleagues, Ian Sherrington, Martin Priest, Ted Smith, and Homer Rahnejat, for useful discussions and suggestions on earlier versions of this manuscript.

References

[1] Phoenix Tribology Ltd, TE 77 high frequency friction machine. https://www.phoenix-tribology.com/at2/leaflet/te77 (accessed 7 May 2026).
[2] PCS Instruments, HFRR. https://pcs-instruments.com/product/hfrr/ (accessed 7 May 2026).
[3] Optimol, SRV—Friction wear testing our synonym with Tribology. https://optimol-instruments.de/en/products/srv5/ (accessed 7 May 2026).
[4] Bruker Corporation, High frequency reciprocating rig module. https://www.bruker.com/en/products-and-solutions/test-and-measurement/tribometers-and-mechanical-testers/high-frequency-reciprocating-rig-module.html (accessed 7 May 2026).
[5] Rtec Instruments, Tribometers: Tribology testing instruments for friction, wear & material analysis. https://rtec-instruments.com/tribometer/ (accessed 7 May 2026).
[6] S. Furuhama, S. Sasaki, Effect of oil properties on piston frictional forces, *Int. J. Vehicle Des.* 7 (1986) 133–150, https://doi.org/10.1504/IJVD.1986.061146.
[7] J.A. McGeehan, A literature review of the effects of piston and ring friction and lubricating oil viscosity on fuel economy, Technical Paper, Warrendale, Society of Automotive Engineers, 780673, 1978.
[8] R. Gohar, Elastohydrodynamics, 2nd ed., Imperial College Press, London, 2001.
[9] A. Cameron, The Principles of Lubrication, Longmans, Green & Co., London, 1966.
[10] S. Furuhama, A dynamic theory of piston-ring lubrication: 1st report, calculation, *Bull. JSME* 2 (1959) 423–428, https://doi.org/10.1299/jsme1958.2.423.
[11] T. Lloyd, The hydrodynamic lubrication of piston rings, *Proc. Inst. Mech. Eng. Conf. Proc.* 183 (1968) 28–34, https://doi.org/10.1243/PIME_CONF_1968_183_276_02.
[12] L.L. Ting, J.E. Mayer Jr, Piston ring lubrication and cylinder bore wear analyses, part II: Theory verification, *J. Lubr. Technol.* 96 (1974) 258–266, https://doi.org/10.1115/1.3451941.
[13] P. Economou, A study of the lubrication and dynamics of piston rings, Doctoral Dissertation, Leeds University, Leeds, 1976.
[14] D. Dowson, Piston assemblies; background and lubrication analysis, in: C.M. Taylor (Ed.), Engine Tribology, Elsevier, Amsterdam, 1993,

pp. 213–240.

[15] Y. Wakuri, M. Soejima, T. Kitahara, M. Nunotani, M. Ootsubo, Studies on the characteristics of piston ring friction, *Trans. JSME Ser. C* 58 (1992) 2293–2298, https://doi.org/10.1299/kikaic.58.2293.

[16] Y.R. Jeng, Theoretical analysis of piston-ring lubrication, part I: Fully flooded lubrication, *Tribol. Trans.* 35 (1992) 696–706, https://doi.org/10.1080/10402009208982174.

[17] R.I. Taylor, Squeeze film lubrication in piston rings and reciprocating contacts, *Proc. Inst. Mech. Eng. Part J J. Eng. Tribol.* 229 (2015) 977–988, https://doi.org/10.1177/1350650114564234.

[18] M.T. Ma, I. Sherrington, E.H. Smith, N. Grice, Development of a detailed model for piston-ring lubrication in IC engines with circular and non-circular cylinder bores, *Tribol. Int.* 30 (1997) 779–788, https://doi.org/10.1016/S0301-679X(97)00036-4.

[19] Y.R. Jeng, Theoretical analysis of piston-ring lubrication part II: Starved lubrication and its application to a complete ring pack, *Tribol. Trans.* 35 (1992) 707–714, https://doi.org/10.1080/10402009208982175.

[20] H.C. Liu, F. Guo, B.B. Zhang, P.L. Wong, Behavior of hydrodynamic lubrication films under non-steady state speeds, *Tribol. Int.* 93 (2016) 347–354, https://doi.org/10.1016/j.triboint.2015.09.026.

[21] L.L. Ting, A review of present information on piston ring tribology, Technical Paper, Warrendale, Society of Automotive Engineers, 852355, 1985.

[22] C. Delprete, A. Razavykia, Piston ring–liner lubrication and tribological performance evaluation: A review, *Proc. Inst. Mech. Eng. Part J J. Eng. Tribol.* 232 (2017) 193–209, https://doi.org/10.1177/1350650117706269.

[23] S.L. Moore, G.M. Hamilton, The piston ring at top dead centre, *Proc. Inst. Mech. Eng.* 194 (1980) 373–381, https://doi.org/10.1243/PIME_PROC_1980_194_044_02.

[24] K. Shin, Y. Tateishi, S. Furuhama, Measurement of oil-film-thickness between piston ring and cylinder, Technical Paper, Warrendale, Society of Automotive Engineers, 830068, 1983.

[25] P.S. Dellis, Effect of friction force between piston rings and liner: A parametric study of speed, load, temperature, piston-ring curvature, and high-temperature, high-shear viscosity, *Proc. Inst. Mech. Eng. Part J J. Eng. Tribol.* 224 (2010) 411–426, https://doi.org/10.1243/13506501JET727.

[26] P.S. Dellis, Aspects of lubrication in piston cylinder assemblies, Doctoral Dissertation, Imperial College, London, 2005.

[27] P.S. Dellis, Oil film thickness measurements combined with high temperature friction investigations in a simplified piston-ring lubrication test rig, *Tribol. Ind.* 41 (2019) 471–483, https://doi.org/10.24874/ti.2019.41.04.02.

[28] H. Nishikawa, K. Handa, M. Kaneta, Behavior of EHL films in reciprocating motion, *JSME Int. J. Ser. C Dyn. Control Robot. Des. Manuf.* 38 (1995) 558–567, https://doi.org/10.1299/jsmec1993.38.558.

[29] L.E. Scales, J.E. Rycroft, N.R. Horswill, B.P. Williamson, Simulation and observation of transient effects in elastohydrodynamic lubrication, Technical Paper, Warrendale, Society of Automotive Engineers, 961143, 1996.

[30] J. Sugimura, W.R. Jones Jr, H.A. Spikes, EHD film thickness in non-steady state contacts, *J. Tribol.* 120 (1998) 442–452, https://doi.org/10.1115/1.2834569.

[31] E. Ciulli, Non-steady state non-conformal contacts: Friction and film thickness studies, *Meccanica* 44 (2009) 409–425, https://doi.org/10.1007/s11012-008-9178-7.

[32] C.J. Hooke, The minimum film thickness in lubricated line contacts during a reversal of entrainment: General solution and the development of a design chart, *Proc. Inst. Mech. Eng. Part J J. Eng. Tribol.* 208 (1994) 53–64, https://doi.org/10.1243/PIME_PROC_1994_208_349_02.

[33] J. Wang, M. Kaneta, P. Yang, Numerical analysis of TEHL line contact problem under reciprocating motion, *Tribol. Int.* 38 (2005) 165–178, https://doi.org/10.1016/j.triboint.2004.07.025.

[34] M.A. Alsamieh, Behavior of elastohydrodynamic lubricating film point contact problems in the unsteady state of reciprocating motion, *World J. Eng.* 22 (2025) 200–217, https://doi.org/10.1108/WJE-09-2023-0321.

[35] M. Priest, R.I. Taylor, D. Dowson, C.M. Taylor, Boundary conditions for Reynolds equation with particular reference to piston ring lubrication, in: Proceedings of the 22nd Leeds-Lyon Symposium on Tribology, Elsevier, Lyon, 1996.

[36] Hand Wiki, Powell's Dog Leg Method. https://handwiki.org/wiki/Powell%27s_dog_leg_method (accessed 7 May 2026).

[37] R.I. Taylor, M.A. Brown, D.M. Thompson, J.C. Bell, The influence of lubricant rheology on friction in the piston ring-pack, Technical Paper, Warrendale, Society of Automotive Engineers, 941981, 1994.

[38] R.I. Taylor, T. Kitahara, T. Saito, R.C. Coy, Piston assembly friction and wear: The influence of lubricant viscometry, in: Proceedings of the International Tribology Conference, Japanese Journal of Tribologists, Yokohama, 1995.

[39] R.I. Taylor, B.R. de Kraker, Shear rates in engines and implications for lubricant design, *Proc. Inst. Mech. Eng. Part J J. Eng. Tribol.* 231 (2015) 1106–1116, https://doi.org/10.1177/1350650117696181.

[40] N.W. Bolander, B.D. Steenwyk, F. Sadeghi, G.R. Gerber, Lubrication regime transitions at the piston ring-cylinder liner interface, *Proc. Inst. Mech. Eng. Part J J. Eng. Tribol.* 219 (2005) 19–31, https://doi.org/10.1243/135065005X9664.

[41] P. Pawlus, R. Reizer, Profilometric measurements of wear scars: A review, *Wear* 534–535 (2023) 205150, https://doi.org/10.1016/j.wear.2023.205150.

[42] M. Priest, D. Dowson, C.M. Taylor, Predictive wear modelling of lubricated piston rings in a diesel engine, *Wear* 231 (1999) 89–101, https://doi.org/10.1016/S0043-1648(99)00125-8.